The double-edged role of FASII regulator FabT in *Streptococcus pyogenes* infection

Clara Lambert[1, †], Caroline Bachmann[1], Marine Gaillard[1], Antoine Hautcoeur[1], Karine Gloux[2], Thomas Guilbert[1], Celine Méhats[1], Bastien Prost[3], Audrey Solgadi[3], Sonia Abreu[4], Muriel Andrieu[1], Claire Poyart[1,5], Alexandra Gruss[2] and Agnes Fouet[1].

[1]Université Paris Cité, Institut Cochin, INSERM, U1016, CNRS, UMR8104, Paris, France; [2]Micalis Institute, INRAE, AgroParisTech, Université Paris-Saclay, Jouy en Josas, France; [3]UMS-IPSIT - Plateforme SAMM, Université Paris Saclay, France ; [4]Lipides: Systèmes Analytiques et Biologiques, Université Paris-Saclay, 91400 Orsay, France.[5]AP-HP Centre–Université Paris Cité, Paris, France.

email: agnes.fouet@inserm.fr ; alexandra.gruss@inrae.fr

[†] Present address : Department of Molecular Biology, Umeå University, Umeå, Sweden

Orcid numbers: A. Fouet, 0000-0001-7715-9157; A. Gruss, 0000-0001-7426-5229; C. Lambert, 0000-0003-2740-1755; T. Guilbert, 0000-0001-5069-0730

Abstract

In *Streptococcus pyogenes*, the fatty acid (FA) synthesis pathway FASII is feedback-controlled by the FabT repressor bound to an acyl-Acyl carrier protein. FabT defects are associated with attenuated virulence in animal models. Nevertheless, *fabT* point mutations arise *in vivo*. To resolve this paradox, we identified conditions and biotopes in which *fabT* behavior is defective, as being human tissues, cells, or cell filtrates. We then defined biotopes in which *fabT* mutants have a growth advantage, as being lipid rich. In a proof of concept we demonstrate that *fabT* mutants emerge in this context, due to FASII derepression, which prevents environmental FA incorporation. Energy dissipation is identified as the principal defect of *fabT* mutants, such that specific nutrients are consumed but do not promote growth. Our findings elucidate the nature of the link between FabT and virulence, provide a rationale for *fabT* mutant emergence, and identify the defect that causes attenuated *fabT* infection.

Introduction

Bacterial membranes form a mutable permeable barrier that facilitates adaptation to a changing environment. They usually comprise a phospholipid bilayer composed of a polar head and apolar fatty acid (FA) chains. The FA synthesis pathway (FASII), which is widespread among bacteria, synthesizes saturated and/or unsaturated FAs joined to an acyl carrier protein (ACP; forming acyl-ACP) (Supplementary Fig. 1a). Unsaturated FAs are produced *via* a FASII shunt catalyzed by an acyl-ACP-isomerase named FabM in streptococci. While FASII is conserved (with some enzyme variation), its regulators differ among Firmicutes. In streptococcaceae and enterococcaccae, FASII gene expression is controlled by a unique MarR-family feedback-type regulator named FabT encoded in the main FASII locus (Supplementary Fig. 1). FabT uses acyl-ACP as corepressor [[1], for review [2]]. Notably, the affinity of FabT-(acyl-ACP) binding to a specific DNA palindromic sequence increases with the length of the acyl carbon chain and the presence of an unsaturation [3]. FabT regulons were characterized in various streptococcaceae species and in conditions that affect membrane FA composition, including growth temperature, pH or growth phase [4-8]. FabT exerts greater repression of genes encoding elongation steps, mainly the *trans*-2-enoyl-ACP reductase II FabK, and less repression of *fabM*. In *Streptococcus pneumoniae fabM* expression is not repressed by FabT [5]. Accordingly, an *S. pneumoniae* strain lacking a functional FabT produced longer and more saturated FAs [5]. FabT regulons reportedly also comprise non-FASII genes involved in transport, DNA and carbohydrate metabolism, protein, purine and pyrimidine synthesis; however, their identities vary according to reports and the species under study [2]. To date, FabT regulons were not analyzed in the presence of exogeneous FAs (eFAs), which enhance FabT transcriptional repression [3]. This missing information is particularly relevant as numerous host infection sites are FA-rich.

Streptococcus pyogenes, also known as Group A *Streptococcus*, GAS, is a major human pathogen responsible for a large variety of clinical manifestations ranging from superficial infections to life-threatening invasive infections. GAS infections rank among the top ten causes of death due to bacterial infections worldwide [9]. GAS isolates mutated in *fabT* were recovered in non-human primates at the point of intramuscular inoculation, raising the possibility of such populations forming in the human host [4]. In a murine model, strains harboring *fabT* point mutations display smaller size lesions, no loss of body weight and a lower mortality than their wild-type counterparts [10]. In a non-human primate model, a *fabT* deleted strain shows decreased colonization and dissemination capacities compared to the parental strain [4]. Its survival is also decreased in human blood or in the presence of human polymorphonuclear leukocytes [4].

These reported properties indicate that the *fabT* mutant variants are poorly adapted for infection, which led us to question the rationale for their emergence. We solve this question here by performing in-depth analyses of the features of WT and a representative *fabT* mutant in different contexts and growth conditions. Conditions are characterized in which *fabT* is deleterious, and the contrary, when it benefits growth. Finally, we show that the *fabT* mutant is metabolically wasteful, which probably contributes to the *fabT* defect during infection. Our findings resolve the apparent contradiction between the *in vivo* emergence of *fabT* variants with reduced virulence and the need for an active FabT repressor during infection.

Results

The WT FabT strain has a fitness advantage over mFabT during growth on human decidua.

Previous observations identified multiple independent FabT point mutants harvested from the infection site of nonhuman primates, some of which mapped to His105 [4]. A strain expressing a $FabT^{H105Y}$ point mutation was constructed in the reference strain M28PF1 (an *emm28* strain, referred to as wild-type; WT) [11,12], here called mFabT. The FabT His105 residue is in the middle of the α5 helix involved in dimerization and acyl-ACP binding (Supplementary Fig. 1b-c) [13]. A *fabT* deletion (Δ*fabT*) mutant was also constructed in the same reference strain.

The mFabT and WT strains grew similarly in both THY and THY supplemented with an exogenous FA (eFA) source (here 0.1 % Tween 80 medium, enriched in C18:1Δ9, oleic acid) (Supplementary Fig. 2a-b). We evaluated the state of WT and $FabT^{H105Y}$ bacteria in mid-exponential phase by live-dead staining (Supplementary Fig. 2c-d). Strain survival was comparable. In contrast to the point mutant, and as previously reported, growth of the *fabT* deletion mutant was defective in laboratory THY medium both in the absence and presence of eFAs (Supplementary Fig. 2e-f) [1,14]. This suggests a broader effect of *fabT* deletion than of *fabT* point mutations as emerge *in vivo*. The relevance of the mFabT point mutant in previous infection studies led us to use this strain for further characterization.

To understand the role of *fabT* and emergence of *fabT* mutants, we designed *ex vivo* assays to study infection with WT and *fabT* variants. mFabT strain capacity to colonize human tissue *ex vivo* was assessed by measuring its growth on human tissue. As *emm28* strains are associated to puerperal fever [15,16], we compared *ex vivo* growth of WT and mFabT on human decidua [17]. In control experiments, both strains failed to grow in RPMI, as assessed by growth ratios between cfus (colony forming units) after 8 h incubation and the inocula (Supplementary

Fig. 2g). In static conditions, growth of the mFabT strain was 63 % lower than that of the WT strain (Fig. 1a). Growth kinetics of WT and mFabT GAS strains were then followed in flow conditions at the tissue surface by time-lapse microscopy (Fig. 1b-c). The surface colonized by the WT strain increased throughout the 4 h growth period (Fig. 1b). In contrast, mFabT strain growth only increased during the first half-hour of image acquisition. The thickness of bacterial microcolonies increased for the WT, but decreased for the mFabT strain (Fig. 1c). Altogether, the WT strain grew with a doubling time of roughly 200 min whereas the mFabT strain did not grow. Thus, in contrast to normal growth in THY medium, the mFabT strain has a major growth defect in the presence of human decidua. These results provide a first insight into the nature of the colonization defect and virulence attenuation of *fabT* mutant strains [4,10].

The mFabT strain displays adhesion and growth defects in the presence of human cells or cell supernatants.

Bacterial colonization of host tissue comprises an initial adhesion step, followed by bacterial multiplication [17]. As GAS has tropism for endometrial and skin tissues, we assessed WT and mFabT adhesion capacities on human endometrial cells, and on differentiated (as present in upper skin layers), and undifferentiated skin keratinocytes (Fig. 1d). The mFabT mutant displayed an adhesion defect on the endometrial cells and undifferentiated keratinocytes compared to the WT. In contrast, the strains adhered similarly on differentiated keratinocytes. The adhesion defect may contribute to the virulence defect observed in the non-human primate animal models [4].

GAS replicates mainly extracellularly during infection of endometrium and skin [18]. We compared growth of WT and mFabT strains on endometrial cells and keratinocytes (Fig. 1e). Growth of the mFabT strain was respectively decreased by 90 %, 53 % and 56 % compared to the WT strain in the presence of endometrial cells, undifferentiated keratinocytes, and

differentiated keratinocytes. The FabT^{H105Y} mutation thus leads to impaired growth in the presence of human cells. To determine whether adhesion is required for the growth differences between WT and *fabT* strains, we assayed bacterial growth in uninfected cell supernatant, termed "conditioned supernatant" (Fig. 1f). The mFabT strain displayed a growth defect in endometrial, undifferentiated and differentiated keratinocyte conditioned supernatants (decreased by 72 %, 50 % and 50 % respectively compared to the WT). This indicates that cell-secreted products differentially affect growth of WT and mFabT strains. Adhesion could nonetheless contribute to promoting higher bacterial densities during infection.

The differences in WT and mFabT growth were visible when grown on endometrial cells or their conditioned supernatants. We therefore consider it likely that endometrial cells secrete the same compounds independently of infection. Higher bacterial growth ratios on differentiated keratinocytes than on the conditioned supernatants may be due to greater nutrient availability after infection. Altogether, these data show that mFabT has both adhesion and growth defects in cell infection environments.

Poor mFabT growth suggests that mFabT makes inefficient use of nutrients secreted by eukaryotic cells and/or is more susceptible than WT to secreted bactericidal molecules. This could lead to slower growth rate, and/or higher bacterial death. We investigated growth kinetics of WT and mFabT strains in endometrial cell conditioned supernatant in time course experiments (Fig. 1g left). Cfu ratios were similar for both strains at 4 h, indicating no difference in the lag time. However, at 8h, cfu ratios were higher for the WT strain (Fig. 1f-g). In addition, mFabT mortality was ~1.5-fold greater than WT at 8 h post-inoculation in conditioned supernatant (Fig. 1g right); these differences were accentuated at 16 h and 24 h (Fig. 1g left). We noted that GAS dies rapidly when growth stops, as seen in RPMI (Supplementary Fig. 2g). We conclude that mFabT grows more slowly and dies more rapidly than the WT strain, and

suggest that GAS death is triggered by slow growth. To elucidate the underlying bases for differential growth of mFabT we resorted to systematic approaches.

Transcriptomes of mFabT *versus* WT vary according to eFA availability.

Transcriptome analyses were performed in the absence of FAs, and also with added FAs (supplied by 0.1 % Tween 80), which activate WT FabT repression (see [2] for Review) (Extended Data Table 1). Pairwise analyses were done as indicated (Fig 2a-d). Results were confirmed by qRT-PCR on chosen genes (Extended Data Table 1; Supplementary Fig. 3a-c and Supplementary Table 1).

In the absence of FAs, FASII genes were comparably expressed in WT and mFabT. However, several differences, often corresponding to multi-gene operons, were observed between the two strains (Extended Data Table 1). Notably, purine synthesis operon genes (M28_Spy0022 to M28_Spy0026) were upregulated in mFabT, suggestive of increased metabolism. An operon encoding adhesins (M28_Spy0107 to M28_Spy0111) was also upregulated in the mFabT strain; however, expression of virulence genes including Mga regulon proteins, the C5 peptidase ScpA, and other adhesins, M protein, Sof and SfbX, was down-regulated (Extended Data Table 1). The defective adhesion of the mFabT strain to endometrial cells and undifferentiated keratinocytes (Fig. 1d) may thus be explained by lower expression of these factors. Altered expression of adhesins and other virulence factors such as SLO and NADase could contribute to the reported poor virulence of this mutant in infection [19].

Addition of FAs activates FabT-mediated repression, which, as expected, leads to repression of FASII gene expression (Fig. 2c, Extended Data Table 1) [3]**.** In contrast, FASII gene expression in the mFabT mutant was unaffected by eFA addition (Fig. 2d, Extended Data Table 1). This result gives clear evidence that the single $FabT^{H105Y}$ mutation, as arises *in vivo*, strongly impairs repressor activity. The effects of mFabT on FASII gene expression were further

examined by qRT-PCR, which is more sensitive than RNAseq. The *fabK*$_{Spy_1481}$ gene displayed ~2-fold greater expression in the mFabT mutant compared to WT (Supplementary Fig. 3a). FabK is involved in FASII synthesis of saturated FAs [2]. Higher *fabK*$_{Spy_1481}$ expression is compatible with a greater proportion of saturated FAs in the mFabT mutant (Supplementary Fig. 1c). Lastly, *degV*$_{Spy_1638}$, not annotated as FASII-related, was more expressed in the mFabT strain, but was repressed in the WT strain grown in Tween (Fig. 2b-c, Supplementary Fig. 3b) [12]. *degV*$_{Spy_1638}$ encodes an FA binding protein, of the FakB-family, which together with FakA constitutes a fatty acid kinase [12,20]. *degV*$_{Spy_1638}$ is the only gene other than those comprising the FASII locus that is preceded by a FabT consensus DNA binding motif (5'-ANTTTGATTATCAAATT; Fig. 2e) [21]. We recently reported that the *degV*$_{Spy_1638}$ gene product is involved in endogenous FA-storage or catabolism [12].

Altogether, these results identify differentially expressed genes in mFabT in the absence of exogenously added FAs. Down-regulation of several adhesins may explain poor mFabT binding to eukaryotic cells (Fig. 1d). They also prove that the single FabT^{H105Y} point mutation loses control of FASII when FAs, required for FabT repression, are supplied. Differences between WT and mFabT in the absence of FAs indicate that intrinsic features differentiate these strains and lead to altered expression. However, these analyses do not explain the *in vivo* emergence of mFabT mutants at an early stage of GAS infection.

mFabT is defective for eFA incorporation.

We analyzed GAS WT and mFabT membrane FA profiles in the absence and presence of eFAs. Without eFAs (Fig. 3a, Extended Data Table 2), the mFabT strain produced markedly higher proportions of saturated FA C18:0 than the WT strain (27 % *vs* 7 %): this is expected as transcription of *fabK* (needed for saturated FA synthesis), but not of *fabM* (needed for unsaturated FA synthesis), is higher in mFabT relative to the WT strain (Supplementary Fig.

3a) [5]. Moreover, the mFabT strain produced longer chain saturated FAs, such that the proportion of C18:0 over the total saturated FAs was 54 % in mFabT and 18 % in WT (Extended Data Table 2). Nevertheless, WT and mFabT strains had similar growth kinetics in laboratory medium (Supplementary Fig. 2a), suggesting that this significant change was not a major determinant for *fabT* mutant emergence.

In the presence of Tween 80, a source of C18:1Δ9, the mFabT mutant contained nearly two-fold less C18:1Δ9 than the WT (30 % compared to 52 % of total FAs, respectively) (Fig. 3b, Extended Data Table 2), suggesting that FA incorporation was defective. In *S. pneumoniae*, a *fabT* mutant reportedly incorporated only traces of unsaturated FAs [5]; in an *Enterococcus faecalis fabT* deletion mutant, incorporation of unsaturated FAs, and to a lesser extent, saturated FAs, was defective [3]. We evaluated FA incorporation by GAS in medium supplemented with C17:1, which is not synthesized by GAS; incorporation of this FA generates a discrete peak by gas chromatography (Fig. 3c left). The proportion of C17:1 was 52 % in the WT strain, and 17 % in mFabT. This confirms that the mFabT strain, in which FASII remains active, has an unsaturated eFA incorporation defect.

We hypothesized that continued FASII synthesis in the mFabT mutant creates competition between endogenously synthesized and eFAs for incorporation into membrane phospholipids. To test this hypothesis, we performed the same experiments in the presence of platensimycin (Fig. 3c right), a FabF inhibitor that blocks FASII synthesis independently of FabT [22]. WT and mFabT strains grew similarly in the presence of C17:1 and platensimycin (Supplementary Table 2), and C17:1 was the major membrane FA in both strains (Fig. 3c).

In conclusion, the $FabT^{H105Y}$ mutant is less responsive to environmental FAs than the WT strain. Poor eFA incorporation in phospholipids is due to continued expression of FASII genes

***De novo* emergence of *fabT* mutants in saturated FA environments.**

We considered that the defect in eFA incorporation could actually confer a growth advantage to the mFabT strain in lipid environments, and thereby point to conditions of *fabT* mutant emergence. Indeed, FA incorporation can negatively affect bacterial integrity, and free FAs are considered part of the first line of host defense against skin infections [23]. Notably, mFabT mutant tolerance for a high proportion of C18:0 in phospholipid membranes (nearly 4-fold increased compared to WT; Fig 3a) led us to examine saturated FAs as potential selective pressure for *fabT* emergence. In pre-screening plate tests, saturated eFAs showed a clear differential toxicity to WT over mFabT (Supplementary Fig. 4). WT and mFabT growth and eFA incorporation were then compared in the presence of C14:0 and C16:0, both of which are found among host lipids [24]. Both FAs inhibited WT growth, and were nonetheless efficiently incorporated in WT membranes; in striking contrast, mFabT failed to incorporate C14:0, and was diminished by >2-fold for C16:0, and strain growth was robust (Fig. 3d-e). This growth advantage incited us to consider that spontaneous *fabT* mutants could emerge in the presence of saturated FAs.

As proof of concept, we grew the WT strain in THY liquid medium without or with C14:0, and then streaked cultures on solid medium containing C14:0 and sequenced the *fabT* genes of emerging colonies. Mutations in *fabT* were obtained in both selection procedures, and encoded FabT variants $FabT^{T64M}$ and $FabT^{G99S}$ (Supplementary Fig. 1b-c). These results provide a rationale for emergence of *fabT* mutants, by generating a growth advantage in lipid-containing biotopes as likely present at the infection locus.

$FabT^{H105Y}$ impacts membrane lipid production and species.

As FAs are major constituents of most bacterial lipids, changes in FA synthesis or incorporation would directly impact lipid composition. We determined how the altered FA distribution and greater FA saturation in mFabT affected membrane lipids. Analyses of lipid contents of WT

and mFabT strains identified three major differences in membrane lipid features (Fig. 4a-b, Extended Data Table 3, Supplementary Fig. 5, Supplementary Table 3): First, the overall lipid content was decreased in mFabT (1.79 mg/mL *versus* 3.06 in the WT as based on equivalent cell mass in THY-grown cultures; Fig. 4a). Second, the proportions of digalactosyldiacylglycerol (DGDG) and cardiolipin (CL) compared to total lipids were notably lower in mFabT (1.7- and 2.8-fold, respectively compared to WT; Fig. 4a). We speculate that the more saturated and longer FAs in mFabT membranes lower lipid membrane synthesis efficiency, which might in turn affect cardiolipin synthesis enzyme activities (Fig. 3a). In favor of this explanation, addition of Tween 80 (C18:1Δ9 source) to the WT strain leads to overall longer membrane FAs (Fig. 3b), and also lowers CL and DGDG levels (Fig. 4a and 4b). Third, deoxy-CL species were increased over 2-fold in mFabT compared to the WT strain (Fig. 4c-e). CL but not deoxy-CL reportedly affects electron transport protein aggregation [25], suggesting physiological relevance to these differences.

Increased FASII activity in the mFabT mutant (Extended Data Table 1) may explain the longer chain FAs comprising CL. Addition of Tween as FA source did not alter the proportions of deoxy-CL and CL species. We conclude that the changes in lipid composition in the mFabT mutant in the absence of eFAs are due to continued FASII activity and greater production of saturated and longer FAs. Lipid species composition, but not their oxidation state, are sensitive to eFA input.

We asked whether the differences in lipid composition between mFabT and the WT strains could explain greater reported resistance of *fabT* mutants to the cationic cyclic peptide polymyxin B (Fig. 4f) [4,26]. We noted that proportions of CL, the polymyxin B membrane target site [26], differed between mFabT and WT strains, and that growth in Tween 80 decreased membrane CL proportions in the WT to those in mFabT when grown without Tween 80. In Tween 80, WT and mFabT showed comparable polymyxin B resistance (Fig. 4f). The

intermediate polymyxin B resistance phenotype of *fabT* mutant strains, like the WT strain grown with eFA, can now be attributed at least in part to the lower levels of CL. We further speculate that *fabT* mutant emergence upon polymyxin B selection [26] is due to their decreased production of CL (Fig. 4a).

Faster metabolic turnover generates a mFabT growth defect during infection.

We investigated a possible metabolic basis for the mFabT growth defect, which could reflect an incapacity to use cell-secreted products for growth, and/or higher mortality (Fig. 1g). To this purpose, we used a metabolomics approach to assess metabolites that are differentially consumed by mFabT compared to the WT strain, as performed on conditioned supernatants. The major classes of detectable compounds that were differentially consumed by WT and mFabT strains were sugars and amino acids (Fig. 5, Extended Data Table 4). Hexoses and amino acids, Asn, Gly, Ile and Lys were the main metabolites overproduced by uninfected cells (Supplementary Fig. 6, Extended Data Table 4). The mFabT strain consumed more hexoses and amino acids Asn, Ile, Lys, and Ser, as seen at 16 h (Fig. 5, Extended Data Table 4). This overconsumption is not linked to a higher bacterial yield, but rather the opposite. These data give evidence that the mFabT mutant has a greater metabolic consumption at the GAS site of infection. Altogether, these data demonstrate that the mFabT strain wastes energy during growth: it over-uses amino acids and hexoses compared to the WT strain, but without growth benefits. Futile energy loss, and expression changes even in the absence of eFAs, can account for the diminished capacity of *fabT* mutants to cause infection.

Discussion

Our work establishes the causal origin for *fabT* mutation emergence and provides an explanation for its disappearance during invasion (Fig. 6): GAS is genetically designed to

incorporate eFA from lipid-containing environments, and repress FASII. We showed that WT GAS growth is inhibited in such environments. Counter-selection can lead to emergence of *fabT* mutants, which have a growth advantage, explaining their detection in a non-invasive infection [4]. The *fabT* mutation would thus confer a selective advantage over non-mutant strains. This was shown here using C14:0 selection; however, we propose that numerous fatty acids would have similar effects. In addition, indirect selective pressures, *e.g.*, *fabT* mutant emergence *via* polymyxin B selection [26], might be explained by their lower CL production (Fig. 4). However, the *fabT* mutation has a cost for virulence: higher mortality and a multiplication defect in the presence of human cells, which is confirmed on human decidua tissue. Continued FASII activity in *fabT* mutant strains provokes a state of futile bacterial metabolism where increased metabolite uptake does not lead to improved growth.

Our findings indicate that futile FASII synthesis by mFabT is detrimental for GAS virulence. We showed previously that blocking FASII with antibiotic inhibitors does not prevent infection by *Streptococcus agalactiae*, nor by other Firmicute pathogens [14,27]. FASII inhibition and eFA incorporation in phospholipids corresponds to the natural feedback inhibition in response to eFAs [2,14]. The contrary, *i.e.*, making FASII synthesis constitutive by inhibiting FabT, is detrimental for *in vivo* infection. FabT could thus be an interesting target for new therapeutics against specific Gram-positive pathogens including GAS, *S. agalactiae*, *E. faecalis,* and *S. pneumoniae*.

Methods

Bacterial strains and culture conditions. The strains used in this study are described in Supplementary Table 4. GAS strains were grown under static condition at 37 °C in Todd Hewitt broth supplemented with 0.2 % Yeast Extract (THY) or on THY agar (THYA) plates. Medium was supplemented with 0.1 % Tween 80 (THY-Tween; Sigma-Aldrich, Ref. P1754) as

indicated, as a source of C18:1Δ9. THY was also supplemented with the saturated FAs, C14:0 and C16:0, in the absence of FA-free bovine serum albumin, 1 $mg.ml^{-1}$ (Sigma-Aldrich, Ref. A6003) Where indicated, the FASII inhibitor platensimycin was added at (1 µg/ml). For strains expressing GFP, medium was supplemented with 10 $\mu g.ml^{-1}$ of erythromycin. For all experiments, strains were prepared as follows. Overnight cultures were diluted to an OD_{600} = 0.05 and grown in THY to the exponential phase (OD_{600} comprised between 0.4 and 0.5). For GFP expression, exponential-phase bacteria were further diluted to OD_{600} = 0.1 in THY supplemented with 10 $\mu g.ml^{-1}$ erythromycin and 20 $ng.ml^{-1}$ anhydrotetracycline, grown for 90 min at 37 °C, and diluted in RPMI as indicated below.

Strain construction. Primers used for clonings and strain verifications are described in Supplementary Table 5. The ΔFabT strain corresponds to a *fabT* deleted mutant. It was obtained by homologous recombination of the plasmid pG1-ΔFabT following a published protocol [28,29]. The DNA fragments encompassing *fabT* were cloned in BamHI – EcoRI digested pG1 using the In Fusion cloning kit® (Clonetech). This led to the deletion of *fabT* from nucleotides 49 to 389, as confirmed by PCR. The mFabT-GFP strain harboring an integrated inducible *gfp* gene was constructed as described for the WT-GFP strain [17]. Whole genome sequencing was performed on the mFabT and mFabT-GFP constructed strains, and no surreptitious mutations were found (Bioproject PRJNA926803, accession number SAMN34247893 for mFabT, SAMN34247911 for mFabT-GFP).

***Ex vivo* GAS growth capacity analysis.** Human placentas with attached maternal-fetal membranes were collected and processed as described [17] with the following modifications. Tissues were obtained after vaginal delivery, and the samples used were from regions located

far from the cervix, known as zone of intact morphology [30]. Human decidual explants were infected within hours of their reception.

Ex vivo bacterial growth capacity in the presence of decidua human tissue was done as follows: exponentially growing GFP-expressing bacteria were washed twice in PBS and diluted in RPMI at a final concentration of 10^4 bacteria per ml. Decidua tissue were washed twice in PBS. One ml of bacteria were then added to tissue, followed by incubation at 37°C + 5 % CO_2. After 8 h, the tissues were shredded using Precellys Evolution (Bertin Technologies) (6 x 20 s at 5500 rpm with a 20 s pause between shaking). Serial dilutions of shredded material were plated on THYA plates. The number of cfus was determined after 24 h of growth at 37 °C and normalized to the inoculum for each experiment.

Live bacterial multiplication on human tissue: infection of maternal-fetal explants, image acquisition and treatments were realized as described [17].

Study approval. The study of the human maternal-fetal membranes was approved by the local ethics committee (Comité de Protection des Personnes Ile de France III, no. Am5724-1-COL2991, 05/02/2013). All participants provided written informed consent prior to inclusion in the study at the Department of Obstetrics, Port Royal Maternity, Cochin University Hospital, Paris, France.

Cell culture. HEC-1-A (ATCC_ HTB-112TM) endometrial epithelial cells were cultured as recommended, in McCoy's 5A medium (Gibco, Ref. 26600080) supplemented with 10 % fetal bovine serum at 37 °C, 5 % of CO_2. HaCaT (Addex-Bio T0020001) keratinocytes were cultivated as recommended, in DMEM high glucose medium (Gibco, Ref. 31966) supplemented with 10 % fetal bovine serum at 37 °C, 5 % of CO_2. HaCaT cells were maintained in the undifferentiated state by cultivation in poor DMEM medium (Gibco, Ref. 21068-028)

supplemented with 1X glutaMax (Gibco, Ref. 35050-038), 1X sodium pyruvate (Gibco, Ref. 11360-039), 2 % fetal bovine serum and 8 % chelated fetal bovine serum using Chelex® 100 Resin (BioRad, Ref. 142-1253). To differentiate HaCaT cells, 2.8 mM $CaCl_2$ (Sigma-Aldrich, Ref. 21115) was added to the medium. Cells were differentiated after seven days as previously described and checked by microscopy [31].

Bacterial adhesion capacity. GAS adhesion capacity was evaluated as described after growing bacteria in THY to an OD_{600} of 0.4 to 0.5 [28]. Values were normalized to the inoculum for each experiment.

Bacterial growth capacity in the presence of eukaryotic cells or culture supernatants. GAS were cultured in THY to OD_{600} = 0.4 - 0.5. Bacteria were washed twice in PBS and diluted in RPMI medium without glutamine (Gibco, Ref. 32404-014) to infect cell cultures or inoculate filtered cell culture supernatants (conditioned supernatants) at a final concentration of 10^3 and 10^4 bacteria per ml, respectively. Confluent cells in 24-well plates were starved 24 h before the experiment, *i.e.* incubated in RPMI medium without glutamine, and washed twice in PBS. Cells were infected with 1 ml of bacteria and incubated at 37 °C + 5 % CO_2. After 8 h, supernatants were recovered and cells were lysed with 1 ml distilled water. The fractions were pooled and serial dilutions plated on THYA plates. Conditioned supernatants were prepared by incubating cells in 1 ml RPMI at 37°C + 5 % CO_2 for 8 h. The conditioned supernatant was recovered, inoculated with 10^3 bacteria, and incubated for another 4, 8, 16 or 24 h. Serial dilutions were plated on THYA plates. The number of cfus was determined after 24 h of growth at 37 °C and normalized to the inoculum for each experiment.

RNA isolation and Illumina RNA-seq sequencing. GAS strains were cultured at 37°C in THY or THY-Tween, and cells were harvested at exponential growth phase (OD_{600} comprised between 0.4 and 0.5). Three independent cultures were prepared for each condition. For RNA preparation, 2 volumes of RNA protect* (Qiagen) was added to cultures prior centrifugation (10 min 12,000 g) and total RNA was extracted from cultures after lysing bacteria by a 30 min 15 $mg.ml^{-1}$ lysozyme, 300 $U.ml^{-1}$ mutanolysine treatment at 20°C followed by two cycles of Fast-prep (power 6, 30 s) at 4 °C. RNA extraction was done using the Macherey-Nagel RNA extraction kit (Germany), as indicated by the supplier. RNA integrity was analyzed using an Agilent Bioanalyzer (Agilent Biotechnologies). 23S and 16S rRNA were depleted from the samples using the MICROBExpress Bacterial mRNA enrichment kit (InVitrogen); depletion was controlled on Agilent Bioanalyzer (Agilent Biotechnologies). Libraries were prepared using an Illumina TS kit. Libraries were sequenced generating 10,000,000 to 20,000,000 75-bp-long reads per sample.

RNA-Seq data analysis. The MGAS6180 strain sequence (NCBI), which is nearly identical to M28PF1 [11,15], was used as a reference sequence to map sequencing reads using the STAR software (2.5.2b) BIOCONDA (Anaconda Inc). RNA-seq data were analyzed using the *hclust* function and a principal component analysis in R 3.5.1 (version 2018-07-02). For differential expression analysis, normalization and statistical analyses were performed using the SARTools package and DESeq2 [32,33] *p*-values were calculated and adjusted for multiple testing using the false discovery rate controlling procedure [34]. We used UpsetR to visualize set intersections in a matrix layout comprising the mFabT *versus* the WT strain grown in THY and in THY-Tween, and growth in THY-Tween *versus* THY for each strain [35,36].

In silico analysis. Geneious prime Biomatters development, www.geneious.com was used to identify 5'-ANTTTGATTATCAAATT-3', the putative FabT binding sequence, on the M28PF1 genome, accepting up to 2 mismatches.

Fatty acid analysis. Strains were grown in THY or THY-Tween until OD_{600} = 0.4 - 0.5. Fatty acids were extracted and analyzed as described [12,14,27,37]. Briefly, analyses were performed in a split-splitless injection mode on an AutoSystem XL Gas Chromatograph (Perkin-Elmer) equipped with a ZB-Wax capillary column (30 m x 0.25 mm x 0.25 mm; Phenomenex, France). Data were recorded and analyzed by TotalChrom Workstation (Perkin-Elmer). FA peaks were detected between 12 and 40 min of elution, and identified by comparing to retention times of purified esterified FA standards (Mixture ME100, Larodan, Sweden). Results are shown as percent of the specific FA compared to total peak areas (TotalChrom Workstation; Perkin Elmer).

Growth curves. GAS stationary precultures were diluted in THY or THY-C14:0 or THY-C16:0 to an OD_{600} = 0.05, transferred to 50 mL falcon tubes, and incubated at 37 °C. Growth was determined by measuring absorbance at 600 nm at different time points.

Spontaneous *fabT* mutants. WT strain overnight precultures were diluted either in THY or in THY-C14:0. When the THY culture reached mid-exponential phase, (OD_{600} = 0.4 - 0.5), both cultures were streaked on THYA supplemented with C14:0 (THYA-C14:0). Plates were incubated 60 h at 37°C. Colonies were isolated on THYA-C14:0, and isolated colonies were subsequently grown on THYA. Six and eight clones originating from the THY and the THY-C14:0 liquid media, respectively, were used for *fabT* sequencing PCR was performed directly

on patched colonies. The oligonucleotides used were FabT-222, and FabTavComp, (Supplementary Table 5) binding 221 bp 5' from the T of the TTG translation start site and 565 bp downstream of it, respectively. The *fabT* gene and surrounding sequences were amplified by PCR using the Green Taq DNA Polymerase, GenScript, according to the manufacturer's instruction, with 30 cycles with a hybridizing temperature of 50°C and an elongation time of 1 min. The Sanger sequencing was carried out by Eurofin Genomics (https://eurofinsgenomics.eu/en/custom-dna-sequencing/portfolio-overview/) on PCR products.

Lipid analysis. Strains were grown in THY or THY-Tween until OD_{600} = 0.4 - 0.5. Cultures were diluted to 7.4 10^7 cfus.mL^{-1}. Lipid extractions and identifications were performed as described [27,38-40]. Lipid separation was realized by normal phase HPLC (U3000 ThermoFisher Scientific) using a Inertsil Si 5µm column (150 x 2.1 mm I.D.) from GL Sciences Inc (Tokyo, Japan). Lipids were quantified using a Corona-CAD Ultra and identified by mass-spectrometry negative ionization and MS^2/MS^3 fragmentations (LTQ-Orbitrap Velos Pro). The concentration of each lipid class was determined as described using as standards DGDG, 840524P-5MG; MGDG, 840523P-5MG; CL (heart CA), 840012P-25MG; PG (egg), 841138P-25MG [41]. Lipid spectra were analyzed on Xcalibur™ software (ThermoFisher Scientific, version 4.2.47).

Polymyxin B assay. Polymyxin B sensitivity was assayed as described [4]. Bacteria were grown to OD_{600} = 0.4 - 0.5 in THY or THY-Tween. Serial dilutions were prepared in PBS, and 2.5 µl of each dilution was inoculated onto THY or THY-Tween plates containing or not 20 µg.ml^{-1} polymyxin B (Sigma-Aldrich, Ref. 81271). Plates were incubated at 37 °C for approximately 24 h and photographed. Experiments were done in biological triplicates.

Live / dead analysis. After bacterial growth in the HEC-1-A conditioned supernatant during 8 h, bacterial Bacterial mortality was determined using the LIVE/DEAD® BacLightTM Bacterial Viability Kit (ThermoFischer Scientific, Ref. L7012) as described for flow cytometry utilization using an ACCURI C6 cytometer (BD Biosciences, Le pont de Claix,France) from the CYBIO Core Facility. Bacteria were grown in HEC-1-A conditioned supernatant for 8 h for testing. Results of three independent experiments were analyzed using the BD Accuri C6 software.

Metabolomic analysis. HEC-1-A conditioned supernatants were inoculated or not with WT or mFabT strains during 8 or 16 h and prepared as described above (see 'Bacterial growth capacity in the presence of eukaryotic cells or culture supernatants'). The metabolite composition of these supernatants was analyzed by Proteigne (https://proteigene.com) using MxP® Quant 500 kit (Biocrates) by two analytical methods, LC-MS/MS for small molecules and FIA-MS/MS for lipids. This analysis was repeated on 3 independent series of supernatants and on RPMI. These analyses have a defined detection threshold (LOD) for each family of metabolite.

Statistical analysis. Data were analyzed with GraphPad Prism version 9.4.1. The tests used are indicated in figure legends. Statistical significance is indicated by: ns (not significant, $p > 0.05$); *, $p < 0.05$; **, $p < 0.01$; ***, $p < 0.001$; ****, $p < 0.0001$.

References

1 Jerga, A. & Rock, C. O. Acyl-Acyl carrier protein regulates transcription of fatty acid biosynthetic genes via the FabT repressor in *Streptococcus pneumoniae*. *J Biol Chem* **284**, 15364-15368, doi:10.1074/jbc.C109.002410 (2009).

2 Lambert, C., Poyart, C., Gruss, A. & Fouet, A. FabT, a Bacterial Transcriptional Repressor That Limits Futile Fatty Acid Biosynthesis. *Microbiol Mol Biol Rev*, e0002922, doi:10.1128/mmbr.00029-22 (2022).

3 Zou, Q., Zhu, L. & Cronan, J. E. The *Enterococcus faecalis* FabT transcription factor regulates fatty acid synthesis in response to exogenous fatty acids. *Front Microbiol* **13**, 877582, doi:doi: 10.3389/fmicb.2022.877582 (2022).

4 Eraso, J. M. *et al.* Genomic Landscape of Intrahost Variation in Group A *Streptococcus*: Repeated and Abundant Mutational Inactivation of the *fabT* Gene Encoding a Regulator of Fatty Acid Synthesis. *Infect Immun* **84**, 3268-3281, doi:10.1128/IAI.00608-16 (2016).

5 Lu, Y. J. & Rock, C. O. Transcriptional regulation of fatty acid biosynthesis in *Streptococcus pneumoniae*. *Mol Microbiol* **59**, 551-566, doi:10.1111/j.1365-2958.2005.04951.x (2006).

6 Eckhardt, T. H., Skotnicka, D., Kok, J. & Kuipers, O. P. Transcriptional regulation of fatty acid biosynthesis in *Lactococcus lactis*. *J Bacteriol* **195**, 1081-1089, doi:10.1128/JB.02043-12 (2013).

7 Faustoferri, R. C. *et al.* Regulation of fatty acid biosynthesis by the global regulator CcpA and the local regulator FabT in *Streptococcus mutans*. *Mol Oral Microbiol* **30**, 128-146, doi:10.1111/omi.12076 (2015).

8 Zhang, J. *et al.* Inactivation of Transcriptional Regulator FabT Influences Colony Phase Variation of *Streptococcus pneumoniae*. *mBio* **12**, e0130421, doi:10.1128/mBio.01304-21 (2021).

9 Carapetis, J. R., Steer, A. C., Mulholland, E. K. & Weber, M. The global burden of group A streptococcal diseases. *Lancet Infect Dis* **5**, 685-694, doi:S1473-3099(05)70267-X [pii] 10.1016/S1473-3099(05)70267-X (2005).

10 Tatsuno, I. *et al.* Relevance of spontaneous *fabT* mutations to a streptococcal toxic shock syndrome to non-streptococcal toxic shock syndrome transition in the novel-type *Streptococcus pyogenes* isolates that lost a salRK. *APMIS* **124**, 414-424, doi:10.1111/apm.12521 (2016).

11 Longo, M. *et al.* Complete Genome Sequence of *Streptococcus pyogenes emm28* Clinical Isolate M28PF1, Responsible for a Puerperal Fever. *Genome Announc* **3**, doi:10.1128/genomeA.00750-15 (2015).

12 Lambert, C. *et al.* A *Streptococcus pyogenes* DegV protein regulates the membrane lipid content and limits the formation of extracellular vesicles. *PLoS One* **18**, e0284402, doi:10.1371/journal.pone.0284402 (2023).

13 Zuo, G. *et al.* Structural insights into repression of the Pneumococcal fatty acid synthesis pathway by repressor FabT and co-repressor acyl-ACP. *FEBS Lett* **593**, 2730-2741, doi:10.1002/1873-3468.13534 (2019).

14 Brinster, S. *et al.* Type II fatty acid synthesis is not a suitable antibiotic target for Gram-positive pathogens. *Nature* **458**, 83-86, doi:10.1038/nature07772 (2009).

15 Green, N. M. *et al.* Genome sequence of a serotype M28 strain of group a streptococcus: potential new insights into puerperal sepsis and bacterial disease specificity. *J Infect Dis* **192**, 760-770, doi:JID33878 [pii] 10.1086/430618 (2005).

16 Plainvert, C. *et al.* Invasive group A streptococcal infections in adults, France (2006-2010). *Clin Microbiol Infect* **18**, 702-710, doi:10.1111/j.1469-0691.2011.03624.x (2012).
17 Weckel, A. *et al. Streptococcus pyogenes* infects human endometrium by limiting the innate immune response. *J Clin Invest* **131**, doi:10.1172/JCI130746 (2021).
18 Pancholi, V. & Caparon, M. in *Streptococcus pyogenes : Basic Biology to Clinical Manifestations* (eds J. J. Ferretti, D. L. Stevens, & V. A. Fischetti) (2016).
19 Zhu, L. *et al.* Contribution of Secreted NADase and Streptolysin O to the Pathogenesis of Epidemic Serotype M1 *Streptococcus pyogenes* Infections. *Am J Pathol* **187**, 605-613, doi:10.1016/j.ajpath.2016.11.003 (2017).
20 Parsons, J. B. *et al.* Identification of a two-component fatty acid kinase responsible for host fatty acid incorporation by *Staphylococcus aureus*. *Proc Natl Acad Sci U S A* **111**, 10532-10537, doi:10.1073/pnas.1408797111 (2014).
21 Rosinski-Chupin, I., Sauvage, E., Fouet, A., Poyart, C. & Glaser, P. Conserved and specific features of *Streptococcus pyogenes* and *Streptococcus agalactiae* transcriptional landscapes. *BMC Genomics* **20**, 236, doi:10.1186/s12864-019-5613-5 (2019).
22 Wang, J. *et al.* Platensimycin is a selective FabF inhibitor with potent antibiotic properties. *Nature* **441**, 358-361, doi:10.1038/nature04784 (2006).
23 Thormar, H. & Hilmarsson, H. The role of microbicidal lipids in host defense against pathogens and their potential as therapeutic agents. *Chem Phys Lipids* **150**, 1-11, doi:10.1016/j.chemphyslip.2007.06.220 (2007).
24 Ni Raghallaigh, S., Bender, K., Lacey, N., Brennan, L. & Powell, F. C. The fatty acid profile of the skin surface lipid layer in papulopustular rosacea. *Br J Dermatol* **166**, 279-287, doi:10.1111/j.1365-2133.2011.10662.x (2012).
25 Haines, T. H. & Dencher, N. A. Cardiolipin: a proton trap for oxidative phosphorylation. *FEBS Lett* **528**, 35-39, doi:10.1016/s0014-5793(02)03292-1 (2002).
26 Port, G. C., Vega, L. A., Nylander, A. B. & Caparon, M. G. *Streptococcus pyogenes* polymyxin B-resistant mutants display enhanced ExPortal integrity. *J Bacteriol* **196**, 2563-2577, doi:10.1128/JB.01596-14 (2014).
27 Kenanian, G. *et al.* Permissive Fatty Acid Incorporation Promotes Staphylococcal Adaptation to FASII Antibiotics in Host Environments. *Cell Rep* **29**, 3974-3982 e3974, doi:10.1016/j.celrep.2019.11.071 (2019).
28 Weckel, A. *et al.* The N-terminal domain of the R28 protein promotes *emm28* group A *Streptococcus* adhesion to host cells via direct binding to three integrins. *J Biol Chem* **293**, 16006-16018, doi:10.1074/jbc.RA118.004134 (2018).
29 Six, A. *et al.* Srr2, a multifaceted adhesin expressed by ST-17 hypervirulent Group B *Streptococcus* involved in binding to both fibrinogen and plasminogen. *Mol Microbiol* **97**, 1209-1222, doi:10.1111/mmi.13097 (2015).
30 Marcellin, L. *et al.* Immune Modifications in Fetal Membranes Overlying the Cervix Precede Parturition in Humans. *J Immunol* **198**, 1345-1356, doi:10.4049/jimmunol.1601482 (2017).
31 Malerba, M. *et al.* Epidermal hepcidin is required for neutrophil response to bacterial infection. *J Clin Invest* **130**, 329-334, doi:10.1172/JCI126645 (2020).
32 Anders, S. *et al.* Count-based differential expression analysis of RNA sequencing data using R and Bioconductor. *Nat Protoc* **8**, 1765-1786, doi:10.1038/nprot.2013.099 nprot.2013.099 [pii] (2013).
33 Varet, H., Brillet-Gueguen, L., Coppee, J. Y. & Dillies, M. A. SARTools: A DESeq2- and EdgeR-Based R Pipeline for Comprehensive Differential Analysis of RNA-Seq Data. *PLoS One* **11**, e0157022, doi:10.1371/journal.pone.0157022 (2016).

34 Benjamini, Y. & Hochberg, Y. Controlling the False Discovery Rate: A Practical and Powerful Approach to Multiple Testing. *J Royal Statistical Society Series B* **57**, 289-300, doi:10.1111/j.2517-6161.1995.tb02031.x (1995).
35 Lex, A., Gehlenborg, N., Strobelt, H., Vuillemot, R. & Pfister, H. UpSet: Visualization of Intersecting Sets. *IEEE Trans Vis Comput Graph* **20**, 1983-1992, doi:10.1109/TVCG.2014.2346248 (2014).
36 Conway, J. R., Lex, A. & Gehlenborg, N. UpSetR: an R package for the visualization of intersecting sets and their properties. *Bioinformatics* **33**, 2938-2940, doi:10.1093/bioinformatics/btx364 (2017).
37 Hays, C. *et al.* Type II Fatty Acid Synthesis Pathway and Cyclopropane Ring Formation Are Dispensable during *Enterococcus faecalis* Systemic Infection. *J Bacteriol* **203**, e0022121, doi:10.1128/JB.00221-21 (2021).
38 Abreu, S., Solgadi, A. & Chaminade, P. Optimization of normal phase chromatographic conditions for lipid analysis and comparison of associated detection techniques. *J Chromatogr A* **1514**, 54-71, doi:10.1016/j.chroma.2017.07.063 (2017).
39 Bligh, E. G. & Dyer, W. J. A rapid method of total lipid extraction and purification. *Can J Biochem Physiol* **37**, 911-917, doi:10.1139/o59-099 (1959).
40 Thedieck, K. *et al.* The MprF protein is required for lysinylation of phospholipids in listerial membranes and confers resistance to cationic antimicrobial peptides (CAMPs) on Listeria monocytogenes. *Mol Microbiol* **62**, 1325-1339, doi:10.1111/j.1365-2958.2006.05452.x (2006).
41 Moulin, M. *et al.* Sex-specific cardiac cardiolipin remodelling after doxorubicin treatment. *Biol Sex Differ* **6**, 20, doi:10.1186/s13293-015-0039-5 (2015).

Acknowledgments

Expert assistance of Benjamin Saint-Pierre (Genom'IC facility of the Institut Cochin) with transcriptomic experiments is gratefully acknowledged. We thank Alice d'Orfani, Lauryn Moali, Iman Nasr and Laure Detheve, undergraduates in the laboratory for technical help, the Imag'IC and Cybio core facilities of the Institut Cochin, and Cédric Broussard, Virginie Salnot and François Guillonneau for helpful discussions. Jamila Anba-Mondoloni (Micalis Institute) provided valuable comments and suggestions on this work, We also thank the personnel of the CIC Mère-Enfant Cochin-Necker for the human decidua. We acknowledge the use of Alphafold and ChimeraX for FabT *in silico* design, and BioRender for computer-generated models.

Funding

CL was supported by Université Paris Cité (BioSPC, n°51809666), FRM (FDT202106012831) and FEMS (FEMS Congress Attendance Grant for poster n° 7875 in 2021 and FEMS grant - LISSSD 2022 n° LISS-213065). This work was supported by DIM One Health (RPH17043DJA) (AF), Agence Nationale de la Recherche (StaphEscape project ANR-16-CE15-0013), and the Fondation pour la Recherche Medicale (DBF20161136769)(AG). IMAG'IC core facility is supported by the National Infrastructure France BioImaging (grant ANR-10-INBS-04).

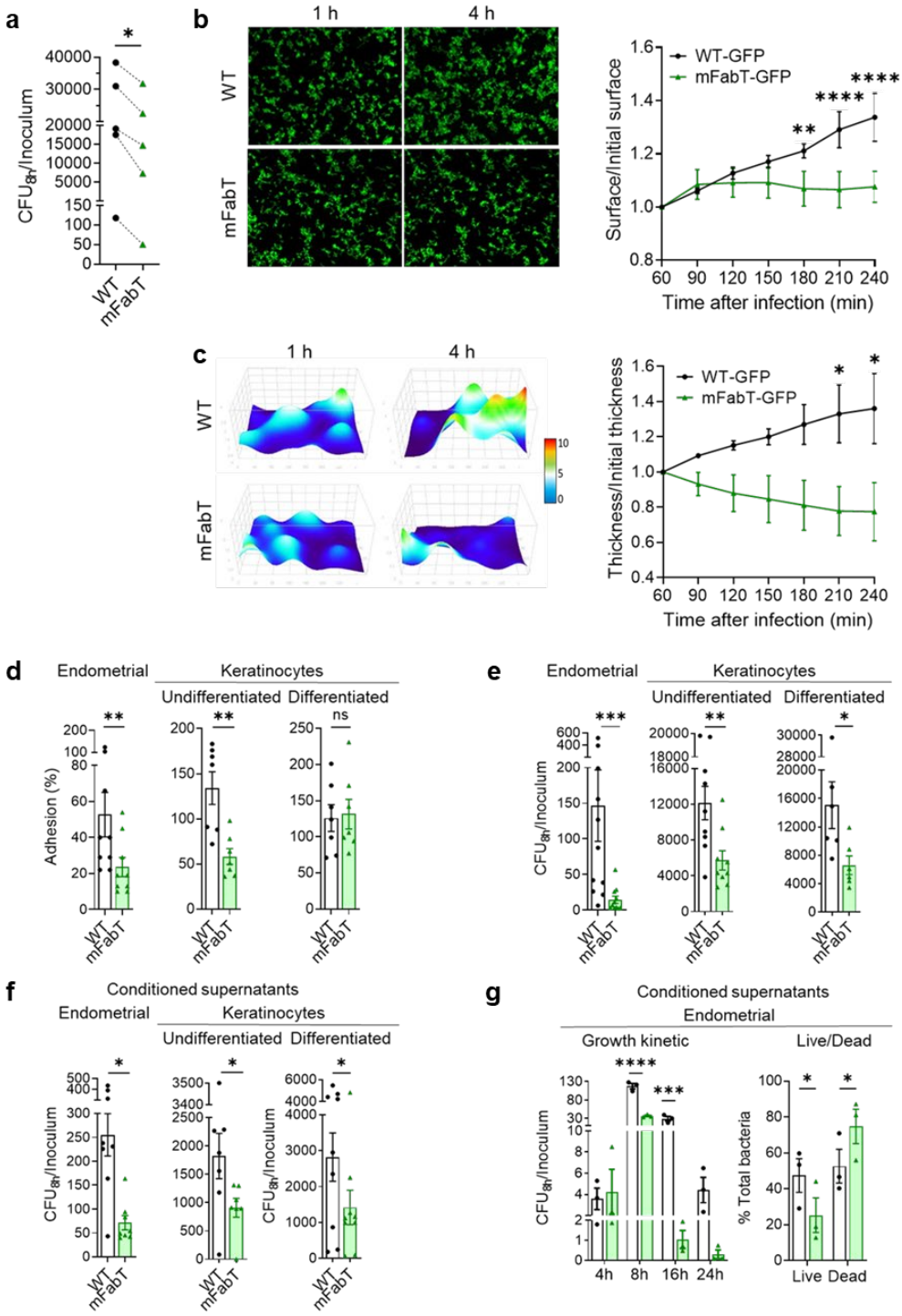

Figure 1 | The mFabT strain grows poorly on human tissue ex vivo and displays adhesion and growth defects in the presence of human cells or in conditioned cell supernatant. a, Comparison of GAS WT and mFabT CFUs after 8 h growth in static conditions in the presence of decidua tissue. **b-c,** Bacterial multiplication at the tissue surface in flow conditions (live imaging); **b, left,** Visualization of WT-GFP and mFabT-GFP multiplication in 2D; **right,** ratios of areas covered by the two strains. **c, left**, 3D-surface heatmap of bacterial layer thickness at 1 and 4 h. The x, y, and z axes are scaled, color code in µm; **right,** ratio over time of thicknesses of WT-GFP and mFabT-GFP strains. **d-g**, Comparison of WT and mFabT strain adhesion and growth capacities in the presence of human cells, or conditioned supernatants. Endometrial cells, undifferentiated keratinocytes, and differentiated keratinocytes, and their respective conditioned supernatants were used as specified. **d**, adhesion ; **e-f,** growth. **g, left,** Bacterial growth kinetics in endometrial conditioned supernatants (cfu.mL-1); **right,** Live/Dead bacteria were assessed after 8 h growth in conditioned supernatants. Growth experiments were started with 10^3 bacteria per ml. Determinations were based on N=5 for **a**, on N=3 for **b**, **c**, **g** and on 6-11 for **d-f**. Analyses were done by T test and Wilcoxon test for **a**, **d-f** and 2-way ANOVA, Bonferroni post-test for **b**, **c**, **g**; *p<0.05; **p<0.01; ***p<0.001; ****p<0.0001. **d-g:** WT, white bars; mFabT, green bars.

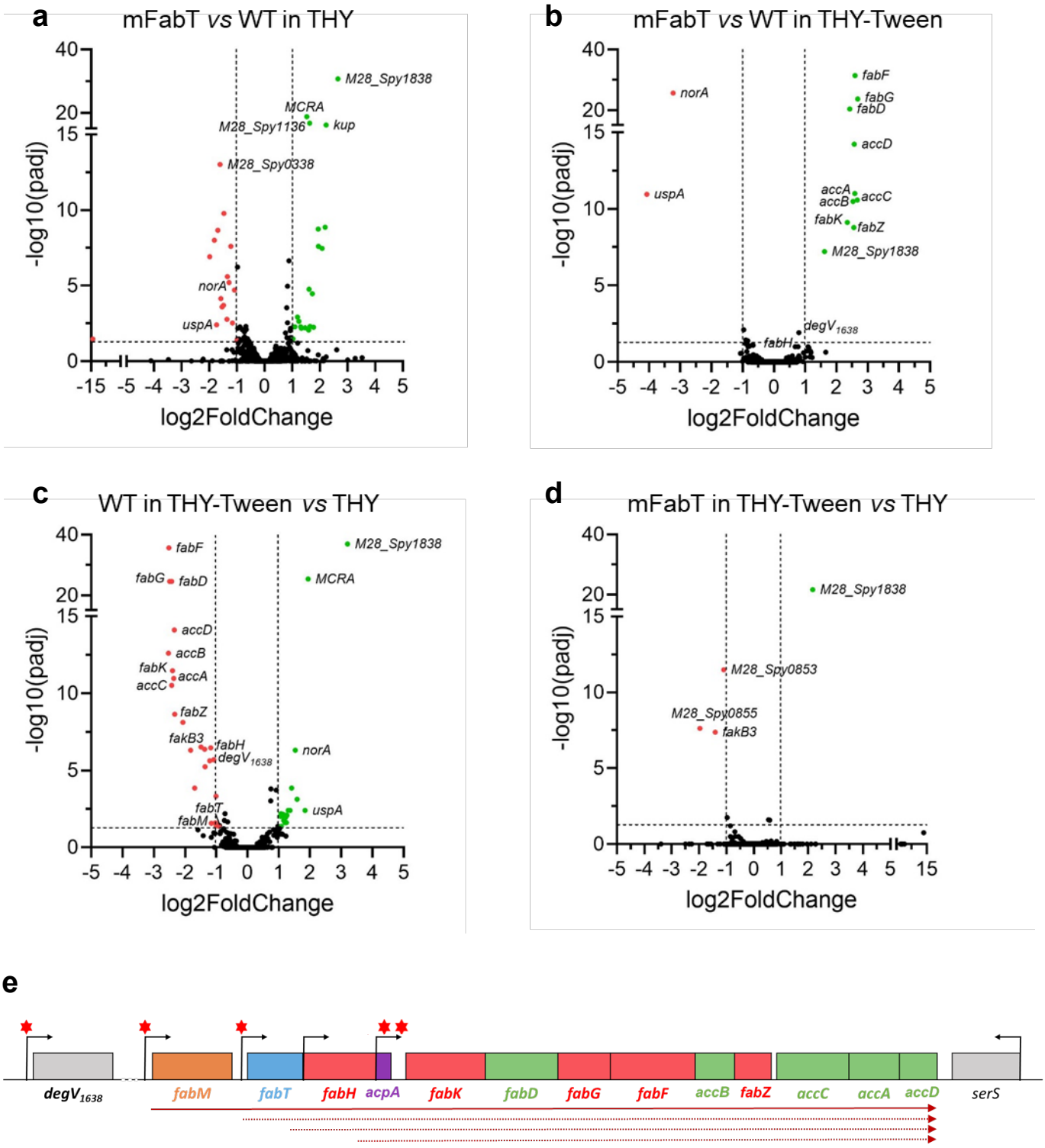

Fig. 2 | FabT regulon in the presence of eFAs and genetic organization of the GAS FASII genes. a-d, Volcano plots of differentially expressed genes, compared as indicated. MCRA, myosin-cross reactive protein encoding an oleate hydratase. Volcano plots were constructed using GraphPad Prism, by plotting the negative base 10 logarithm of the p value on the y axis, and the log of the fold change (base 2) on the x axis. The p-values for comparisons of the peak intensity were calculated by t-tests. Padj: calculated p-values were adjusted for multiple testing using the false discovery rate controlling procedure (see Methods section). Data points with low p values (highly significant) appear toward the top of the plot. **e**, Schematic representation of GAS FASII locus and *degV* gene. Gene positions with names below are represented. Red asterisks, putative FabT binding sites; bent arrows, transcription start sites; solid arrow, transcript defined by RT-PCRs; dotted arrows, transcripts [21].

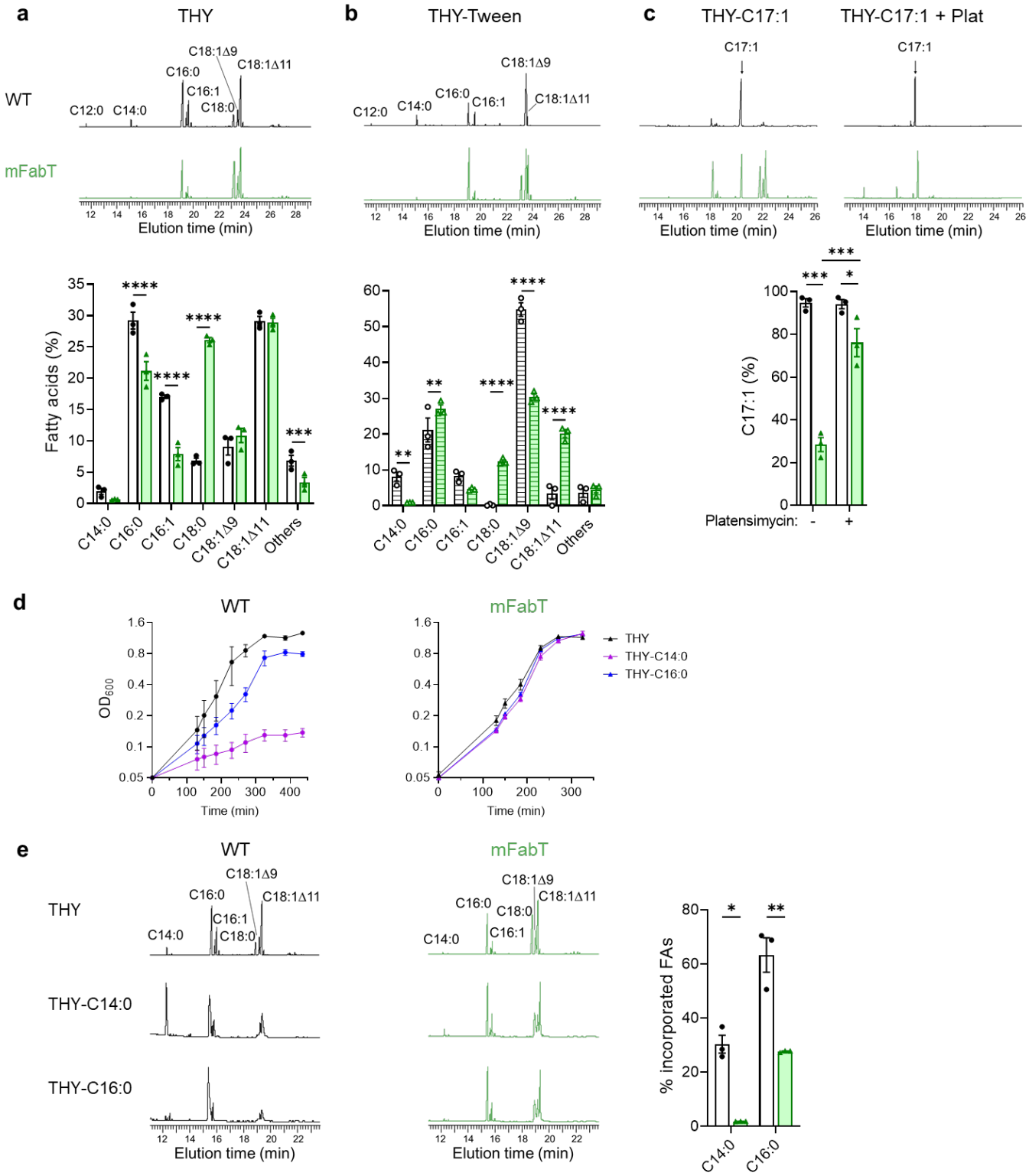

Fig. 3 | The eFA incorporation defect of the mFabT strain confers a selective advantage in certain lipid environments. a, b, c, FA membrane composition of WT and mFabT strains grown in the indicated media supplemented or not with FAs and the FASII-inhibitor platensimycin (1 μg/mL^{-1}) as indicated. Upper, FA profiles; lower, quantified proportions of major FAs. **d**, Growth of WT (left), and mFabT (right) in THY supplemented with 100 μM saturated FAs, C14:0 or C16:0. **e, Left,** Incorporation of exogenous C14:0 and C16:0 from cultures described in '**d**'. **Right**, Quantified percentages of C14:0 and C16:0 incorporation from growth experiments at left. For these analyses, N = 3, 2-way ANOVA, Bonferroni post-test, *p<0.05; **p<0.01; ***p<0.001; ****p<0.0001. WT (black lines, white bars) and mFabT (green lines and bars).

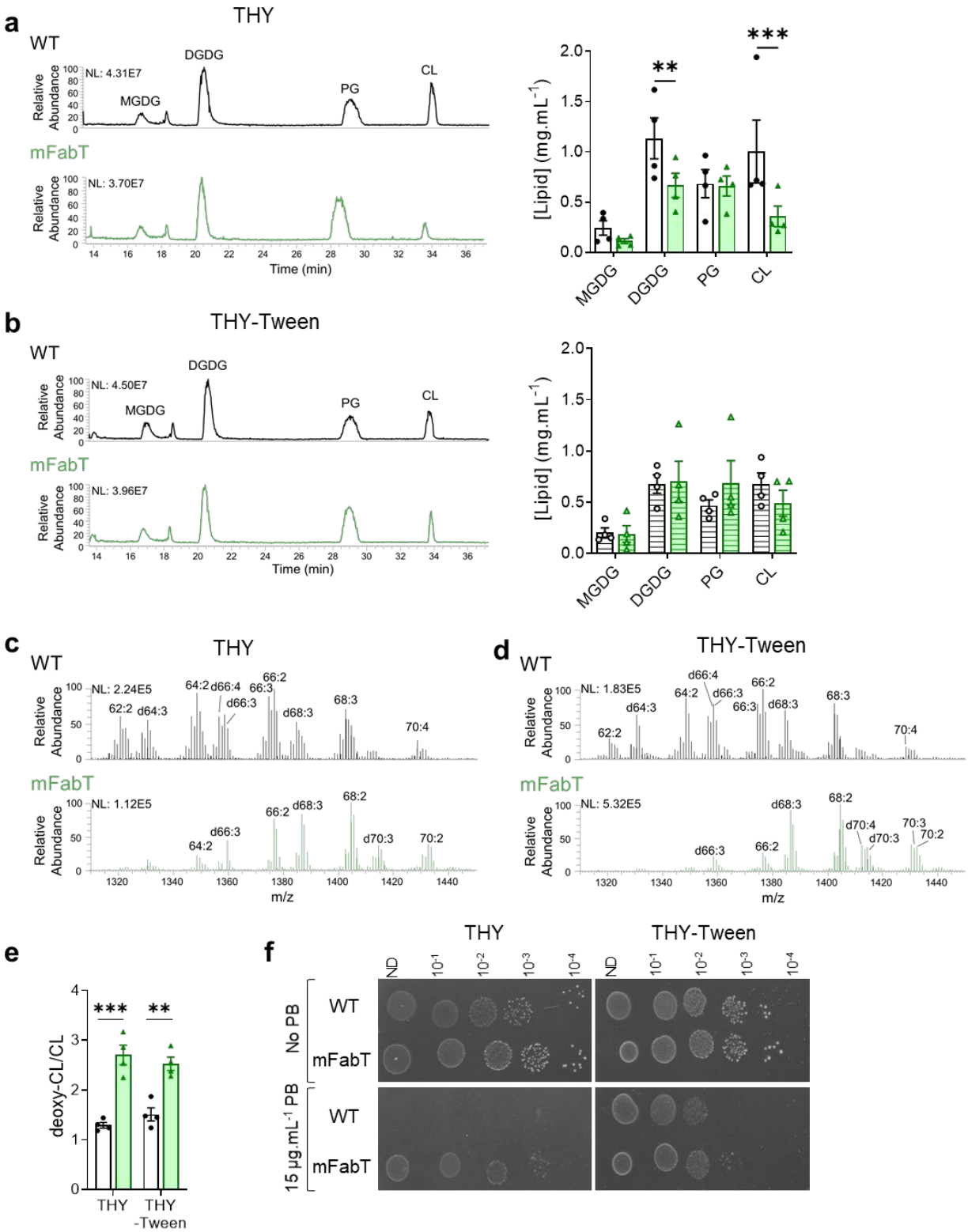

Fig. 4 | FA differences in WT and mFabT strains impact lipid content and composition. a, b, HPLC-MS profiles represent the main lipid classes in strains grown in indicated media; upper, lower, lipid profiles and quantifications by class. WT, black lines, white bars; mFabT, green lines and bars. Lipid concentrations (per mL) correspond to 7.4×10^7 cfus. MGDG, monogalactosyldiacylglycerol; DGDG, digalactosyldiacylglycerol; PG, phosphatidylglycerol; CL, cardiolipin (Extended Data Table 3). **c, d, e** CL species in WT and mFabT, showing deoxy-CL species (indicated by a d preceding the mass; see Extended Data Table 3); **a-b,** N=4; **c-d,** N=3. **a, b, e,** 2-way ANOVA, Bonferroni post-test,; **p<0.01; ***p<0.001; ****p<0.0001 **f,** Polymyxin B sensitivity. WT and mFabT were precultured to OD_{600} = 0.5 in THY or THY-Tween 80 and dilutions were spotted on the same solid medium supplemented or not with polymyxin B (PB). Plates are representative of 3 independent experiments. Strains were grown in THY (open bars) and THY-Tween (hatched bars). **a-d**, NL, normalization level; WT, white bars; mFabT, green bars.

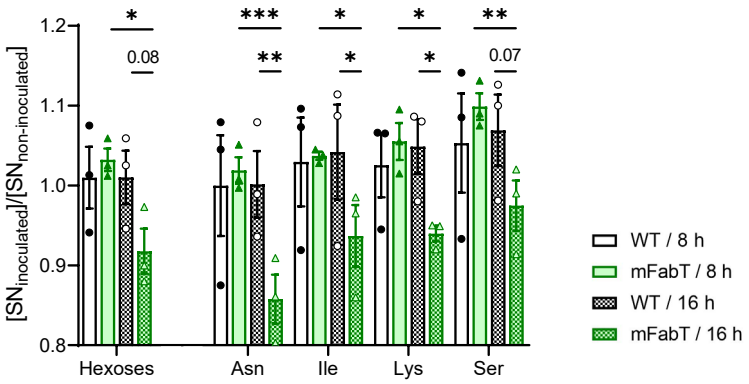

Fig. 5 | The mFabT strain is more energy-consuming than the WT strain. Metabolomic analysis of conditioned supernatants and conditioned supernatants inoculated with WT or mFabT after 8 or 16 h incubation. Carbohydrate and amino acid consumption by the mFabT strain (also see **Extended data Table 6**). N = 3, 2-way ANOVA, Bonferroni post-test; *p<0.05; **p<0.01; ***p<0.005; p-values just above the p= 0.05 threshold are indicated. Strains and growth times are at right.

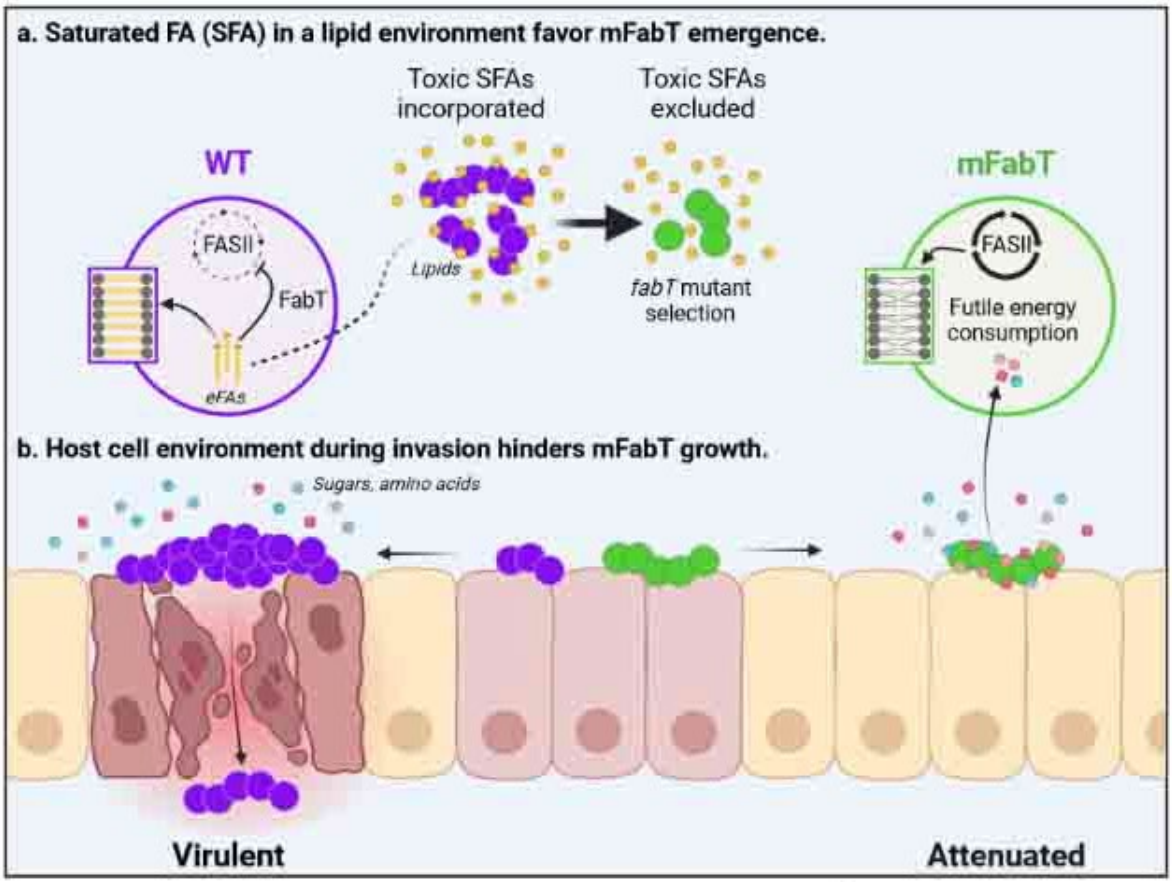

Fig. 6 | Model for emergence of *fabT* mutants that are attenuated for virulence. a, Saturated FAs (SFA) in a lipid environment favor mFabT emergence. Toxic FAs may be present in initial GAS contacts with the host. Counter-selection would lead to emergence of FA-insensitive *fabT* mutants, conferring a growth advantage. In a proof of concept, we show that *fabT* mutants are selected in an SFA environment. **b, Host cell environment during invasion hinders mFabT growth**. Compared to the WT, *fabT* mutant bacteria fail to develop and die more rapidly when exposed to human cells; they are also impaired for adhesion (**Fig. 1**). Continued FASII activity in *fabT* mutants provokes a state of futile bacterial metabolism where metabolite uptake is stimulated, but does not lead to improved growth. Thus, *fabT* mutants in GAS populations may confer a survival advantage during initial infection, but do not withstand host cell infection conditions. Mauve and green circles, WT and mFabT cocci; zoom is on phospholipids. Small yellow circles and lines, lipids and eFA hydrolysis products respectively, small red, blue, pink circles, sugars and amino acid residues. Figure was drawn using BioRender (BioRender.com).